A Unified Probabilistic Approach for Modeling Trajectory-based Separations

Jing Wei and Matthew J. Realff
School of Chemical and Biomolecular Engineering, Georgia Institute of Technology, Atlanta, GA 30332

DOI 10.1002/aic.10509
Published online June 20, 2005 in Wiley InterScience (www.interscience.wiley.com).

The traditional approach to modeling solid–solid separations is based on solving differential equations for particle concentration profiles. This approach is difficult to generalize when the particle properties, such as size and charge, are random variables. If we view particle trajectories as the ultimate differentiating factor, and the nonsharpness of separation as a result of the existence of various random variables such as the random particle properties, and random velocities caused by such phenomena as hydrodynamic interactions, then the recovery can be modeled as a joint probability of particles reaching a certain separation boundary. It is shown that the probabilistic model is a unified approach for various trajectory-based particle separations including sink-float, froth flotation, and electrostatic separation. We transform the recovery models, which have various forms, to the single-form partition curve model that can simplify the design. The design procedure is reduced to optimally setting two model parameters by adjusting the design and operating variables. © 2005 American Institute of Chemical Engineers *AIChE J,* 51: 2507–2520, 2005

Keywords: modeling, design, solids separation, stochastic process, joint cumulative distribution function, sink and float, froth flotation, electrostatic separation

Introduction

Mechanical separation of solids is of growing importance in the domain of recycling processes, such as in the separation of a mix of different plastics.[1] The differences in various particle properties such as density, size, and charge are used for separation design. Unlike equilibrium-based separations, such as distillation and adsorption, the particle trajectory is the ultimate differentiating factor in mechanical separation of solid particles. However, the trajectory is usually not a constant, even for identical particles, as a result of hydrodynamic interactions and random initial conditions. Moreover, there exist distributions of particle properties caused by preprocessing units. For example, size reduction units such as a shredder or a grinder generate a particle size distribution[2] and charging devices such as a rotating drum or a fluidized bed produce a wide charge distribution.[3] Thus separations are usually nonsharp.

The inspiration for many of the recycling separation methods is the mineral processing industry, where mechanical separations are widely used. For many of the mineral processing steps, an S-shaped partition curve (Figure 1) is a common representation of the separation efficiency.

Although many forms of mathematical functions[4] have been used to fit the curve, there are usually two parameters: one for the curve position such as the pivoting point, another for the slope of the curve. For example, the logistic function is of the following form

$$R = \frac{1}{1 + \exp\left[\dfrac{1.0986}{Ep}(\beta - \beta_{50})\right]} \tag{1}$$

where Ep is the probable error [$=(\beta_{25} - \beta_{75})/2$], and β_{75}, β_{50}, and β_{25} denote the particle properties corresponding to 75, 50,

Correspondence concerning this article should be addressed to M. J. Realff at matthew.realff@che.gatech.edu

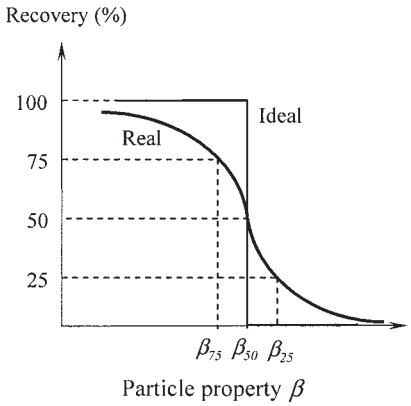

Figure 1. Partition curve.

and 25% recovery, respectively. Therefore, *Ep* represents the separation efficiency. Various empirical equations have been proposed for *Ep* and β_{50} as functions of design and operating variables for different separation methods.

Usually the experimental data are obtained by varying the material property, but in each experiment the property is a constant. In other words, the empirical equation cannot be used if the feed material property has a distribution. In such a case, one needs the position of the curve to be represented as a function of the mean value of the property, with the variance information captured in the *Ep* value. Such empirical relationships have not been presented in the literature to date, and it is the purpose of this paper to present a systematic methodology for their construction and use in a design procedure.

If an approach based on first principles is used to develop a model then the usual starting point is to pose and solve differential equations for the particle concentration profile, in the following three scenarios:

(1) For solids sedimentation in liquids: an axial dispersion model for particle concentration profiles $C(t, y)$

$$\frac{\partial C}{\partial t} = \frac{\partial}{\partial y}\left(D\frac{\partial C}{\partial y}\right) - \frac{\partial}{\partial y}(vC) \tag{2}$$

where D is the diffusion coefficient and v is the settling velocity.

(2) For the elutriation of fines in gas fluidized beds[5]: a first-order ordinary differential equation (ODE) for the concentration at the exit

$$\frac{\partial C}{\partial t} = -kC \tag{3}$$

where k is a rate constant

(3) For column flotation[6]: a combination of the two

$$\frac{\partial C}{\partial t} = \frac{\partial}{\partial y}\left(D\frac{\partial C}{\partial y}\right) - \frac{\partial}{\partial y}(vC) - kC \tag{4}$$

When there is a distribution of particle property, such as the particle size, individual particles with different sizes would have different settling velocities. Thus, even if the diffusion coefficient can be assumed constant, the concentration profile cannot be obtained through solving a single differential equation because of the distribution of settling velocities.

The major reason that causes both approaches (empirical correlations and the differential equations of concentration) to fail is that they are macroscopic methods that do not reveal the real separation mechanisms. It has been shown experimentally that long-time behavior of the sedimentation velocity variance is characteristic of a diffusion process.[7-9] This can also be verified mathematically through the transformation of a Fokker–Planck equation to a stochastic differential equation (SDE).[10] Therefore, if we can attain a trajectory model for a single particle, the recovery is the probability of the stochastic particle trajectories reaching a certain separation boundary. Thus, we can model situations where distributions of particle properties and hydrodynamic interactions coexist. We will illustrate this through several different applications.

Another objective of this article is to build a connection between the partition curve model (Eq. 1) and the recovery model derived from probabilistic considerations. Recovery models for different separation methods have taken many forms, but the partition curve model has a general form. Thus, if explicit relationships of *Ep* and β_{50} with the random variables as well as other deterministic design and operating variables can be determined from the probabilistic approach, we can easily find which parameters should be adjusted to achieve the required separation efficiency. This will allow a significantly more systematic approach to the design of these systems to be taken.

The article is organized as follows. The next section is a motivating example (sink-float sedimentation). In the next section we propose the unified probabilistic approach. The following section includes several applications for which we will skip the derivations and state only the results; the next section is an analysis of a simple design procedure followed by the conclusion. A detailed derivation of the froth flotation model is presented in the Appendix.

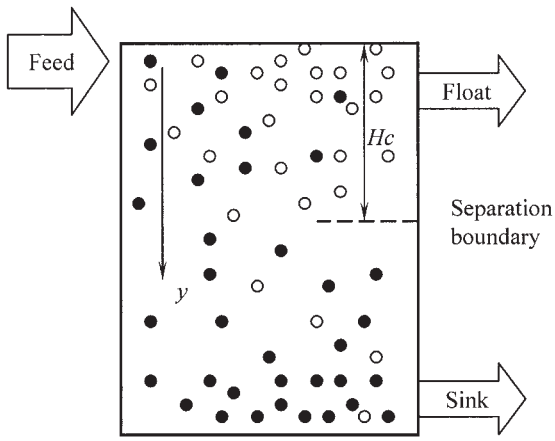

Figure 2. Schematic of a sink-float tank.

A Motivating Example (Sedimentation in Sink-Float Tank)

In this section, we consider particle sedimentation in a sink-float tank (Figure 2) in which the particle size distribution and hydrodynamic diffusion cause the particle trajectories to exhibit random perturbations. The separation is mainly based on the difference of particle density, although particle size also has an influence on the settling velocity. It is assumed that particles that do not settle below the separation boundary Hc, within residence time τ, will report to the overflow.

Consider a case where the particle size is normally distributed with mean μ_{dp} and standard deviation σ_{dp}. It is assumed that particles are spherical, diffusion coefficient D is a constant, and particles quickly reach their terminal velocity. Also assume the flow is in the turbulent region (drag coefficient $C_d = 0.44$), so we have for the terminal velocity

$$\nu_\infty = \beta\sqrt{3.03 g \mu_{dp}} \tag{5}$$

$$\beta = \text{sign}(\rho_p - \rho_l)\sqrt{\left|\frac{\rho_p - \rho_l}{\rho_l}\right|} \tag{6}$$

where

$$\text{sign}(x) = \begin{cases} 1, & \text{if } x \geq 0 \\ -1 & \text{if } x < 0 \end{cases}$$

and ρ_p and ρ_l are solid and liquid densities, respectively.

One can start from a particle level view and describe the system using SDEs. It has been shown that the sedimentation process is well represented by a Markov process that is the solution of the following SDE[9]:

$$dY_t = \nu_\infty dt + B dW_t \tag{7}$$

where Y_t is the particle vertical position at time t, $D = B^T B$, and W is a vector of independent Wiener processes. The Wiener process is a continuous-time stochastic process for $t \geq 0$ with $W(0) = 0$, such that the increment $W(t) - W(s)$ is Gaussian with mean 0 and variance $(t - s)$ for any $0 \leq s < t$, and increments for nonoverlapping time intervals are independent. Brownian motion is the most common example of a Wiener process. The first term on the right-hand side of Eq. 7 describes a deterministic settling of a particle in a infinite dilute suspension and the second term accounts for the velocity fluctuations caused by particle-particle interactions. Each particle moves independently, in each time step, according to the stochastic process defined by Eq. 7.

The SDE can be solved by discretizing the time τ into N intervals (each Δt) and the space variable

$$Y(t + \Delta t) = Y(t) + \nu_\infty \Delta t + \sqrt{2D\Delta t}\,\psi \tag{8}$$

where ψ is a random number from the standard normal distribution $N(0, 1)$. Because $\sum_{i=1}^{n} \Delta t = n\Delta t = \tau$, $\sum \psi \sim N(0, \sqrt{n})$, we have $\sqrt{2D\Delta t}\sum \psi \sim N(0, \sqrt{2D\tau})$. After adding a series of Eq. 8 from $Y(0)$ to $Y(\tau)$, and assuming $Y(0) = 0$, we have

$$Y(\tau) \sim N(\nu_\infty \tau,\ \sqrt{2D\tau}) \tag{9a}$$

or

$$\nu = Y/\tau \sim N(\nu_\infty,\ \sqrt{2D/\tau}) \tag{9b}$$

Thus, the diffusion process corresponds to a stochastic process with mean velocity v_∞ and standard deviation $\sqrt{2D/\tau}$.

The relationship in Eq. 9 is a trajectory model that can be used to derive the recovery model. The recovery is the fraction of particles whose final vertical positions $Y(\tau)$ are no larger than the separation boundary position Hc.

$$\Pr\{Y \leq Hc\} = \Pr\{\beta\sqrt{3.03 g dp}\,\tau + B \leq Hc\} \tag{10}$$

where $B \sim N(0, \sqrt{2D\tau})$.

For reasons of exposition, we assume that particle size dp has an influence only on the mean settling velocity but not on the variance of velocity (that is, D is independent of dp); therefore, the distributions of particle size dp and B are independent. The recovery is a joint probability

$$R = \int_0^\infty \int_{-\infty}^{Hc - \beta\tau\sqrt{3.03 g dp}} \times \left\{ \frac{\exp\left[-\frac{1}{2}\left(\frac{B}{\sqrt{2D\tau}}\right)^2\right]}{\sqrt{2\pi}\,\sqrt{2D\tau}} \frac{\exp\left[-\frac{1}{2}\left(\frac{d_p - \mu_{dp}}{\sigma_{dp}}\right)^2\right]}{\sqrt{2\pi}\,\sigma_{dp}} \right\} \times dB dd_p \tag{11}$$

It is impossible to derive an analytical formula for the joint probability. Therefore, a numerical calculation of Eq. 11 was performed to fit the following empirical model

$$Ep = Ep_1 + Ep_2 - \frac{c_{12}}{\left(1 + \frac{a_{12}}{Ep_1}\right)\left(1 + \frac{b_{12}}{Ep_2}\right)} \tag{12}$$

where a_{12}, b_{12}, and c_{12} are constants, and Ep_1 and Ep_2 are the Ep values of cases where only the first random variable (velocity) or the second random variable (size) exists, respectively.

We choose this form of the model because it satisfies the general requirements:

(1) $Ep \to Ep_2$, as $Ep_1 \to 0$.

(2) $Ep \to Ep_1$, as $Ep_2 \to 0$.

There might be some other forms that also satisfy the above requirements, such as

$$Ep = Ep_1 + Ep_2 - a_{12} Ep_1^{b_{12}} Ep_2^{c_{12}}$$

However, practical calculations in a number of applications indicated that this form is worse than that in Eq. 12.

First, we determine β_{50}. Physically, a particle whose settling velocity and size are at their mean values will exactly reach the separation boundary Hc when its β value equals β_{50}. This

Table 1. Ranges of Parameter and Variable Values in Regression for Sink-Float Separations

Hc (m)	0.1–2.0	D(m^2/s)	0.002–0.200
τ (s)	1–60	μ_{dp} (m)	0.004–0.015
		σ_{dp} (m)	0.001–0.004

provides a way to determine β_{50} by letting $\beta\sqrt{3.03gdp}\tau + B = Hc$ with dp and B at their respective mean values (that is, μ_{dp} and 0). Therefore

$$\beta_{50} = \frac{Hc/\tau}{\sqrt{3.03g\mu_{dp}}} \tag{13}$$

Next, we derive the expressions for Ep_1 and Ep_2, respectively.

(1) For Ep_1, there is only a velocity distribution, and particle size is constant.

From Eq. 9, we have

$$R = \Pr\{Y \le Hc\} = \frac{1}{2}\left[1 + \text{erf}\left(\frac{Hc/\tau - \nu_\infty}{\sqrt{2}\ \sqrt{2D/\tau}}\right)\right] \tag{14}$$

To find the expressions for Ep from Eq. 14, let $R = 0.75$ and 0.25; then we have, respectively,

$$\frac{Hc/\tau - \nu_\infty}{\sqrt{2}\ \sqrt{2D/\tau}} = 0.4769 \qquad \text{and} \qquad \frac{Hc/\tau - \nu_\infty}{\sqrt{2}\ \sqrt{2D/\tau}} = -0.4769$$

$$\beta_{75} = -\frac{0.6745\sqrt{2D/\tau}}{\sqrt{3.03g\mu_{dp}}} + \frac{Hc/\tau}{\sqrt{3.03g\mu_{dp}}} \tag{15}$$

$$\beta_{25} = \frac{0.6745\sqrt{2D/\tau}}{\sqrt{3.03g\mu_{dp}}} + \frac{Hc/\tau}{\sqrt{3.03g\mu_{dp}}} \tag{16}$$

Thus

$$Ep_1 = \frac{\beta_{25} - \beta_{75}}{2} = \frac{0.6745\sqrt{2D/\tau}}{\sqrt{3.03g\mu_{dp}}} \tag{17}$$

(2) For Ep_2 there is only a size distribution and there is no hydrodynamic diffusion.

$$R = \frac{1}{2}\left[1 + \text{erf}\left(\frac{\dfrac{Hc^2}{3.03g\tau^2\beta^2} - \mu_{dp}}{\sqrt{2}\ \sigma_{dp}}\right)\right] \tag{18}$$

Using a procedure similar to that in (1), we have

$$Ep_2 = \frac{Hc(\sqrt{\mu_{dp} + 0.6745\sigma_{dp}} - \sqrt{\mu_{dp} - 0.6745\sigma_{dp}})}{2\tau\sqrt{3.03g}\ \sqrt{\mu_{dp}^2 - 0.455\sigma_{dp}^2}} \tag{19}$$

Once we have the recovery model under either case, we have an alternative way to find β_{50}. By letting Eq. 14 or Eq. 18 equal 0.5, we reach the same expression as in Eq. 13.

With expressions for Ep_1 and Ep_2, we are now ready to fit the Ep values to the model in Eq. 12. Values of design variables (Hc, τ) and distribution parameters (D, μ_{dp}, σ_{dp}) are varied within the ranges shown in Table 1 to obtain a number of Ep values.

The least-squares method is used and the values of the coefficients are $a_{12} = 0.1446$, $b_{12} = 0.0387$, $c_{12} = 0.1866$, with root mean squared error (RMSE) = 0.0029 and relative root mean squared error (RRMSE) = 3.03%.

We have thus obtained a recovery model (Eqs. 1, 12, 13, 17, and 19) for solids sedimentation in a sink-float tank.

A Unified Probabilistic Approach for Trajectory-based Separations

The unified probabilistic modeling approach is a microscopic view of the separation problem in which the nonsharpness is caused by random effects, especially the particle properties, represented as random variables with known distributions. The motivating example above suggests a three-step approach:

(1) Modeling the single-particle trajectory based on the force balance and other first-principles modeling.

(2) Modeling the recovery based on a probability calculation.

(3) Deriving expressions for Ep and β_{50} for the partition curve model.

Often obtaining an analytical solution of the particle trajectory and/or an analytical formula for the probability integral is not possible. In this case, a numerical solution of the differential equation and/or a numerical integration is necessary.

β_{50} can be derived from the corresponding deterministic case. For the Ep value, when one only has numerical solutions of the probability integral, one can use the following empirical model

$$Ep = Ep_1 + Ep_2 + \cdots Ep_n - \sum\sum_{i_1<i_2} \frac{c_{i_1i_2}}{\left(1 + \dfrac{a_{i_1i_2}}{Ep_{i_1}}\right)\left(1 + \dfrac{b_{i_1i_2}}{Ep_{i_2}}\right)}$$

$$- \sum\sum\sum_{j_1<j_2<j_3} \frac{g_{j_1j_2j_3}}{\left(1 + \dfrac{d_{j_1j_2j_3}}{Ep_{j_1}}\right)\left(1 + \dfrac{e_{j_1j_2j_3}}{Ep_{j_2}}\right)\left(1 + \dfrac{f_{j_1j_2j_3}}{Ep_{j_3}}\right)}$$

$$- \cdots - \sum\sum\cdots\sum_{k_1<k_2<\cdots<k_n}$$

$$\times \frac{s_{k_1k_2\cdots k_n}}{\left(1 + \dfrac{p_{k_1k_2\cdots k_n}}{Ep_{k_1}}\right)\left(1 + \dfrac{q_{k_1k_2\cdots k_n}}{Ep_{k_2}}\right)\cdots\left(1 + \dfrac{r_{k_1k_2\cdots k_n}}{Ep_{k_n}}\right)} \tag{20}$$

where Ep_i is the Ep value when only the ith random variable exists and $a_{i_1i_2}$, $b_{i_1i_2}$, $c_{i_1i_2}$, $d_{j_1j_2j_3}$, $e_{j_1j_2j_3}$, $f_{j_1j_2j_3}$, $g_{j_1j_2j_3}$, ..., $p_{k_1k_2\cdots k_n}$, $q_{k_1k_2\cdots k_n}$, ..., $r_{k_1k_2\cdots k_n}$, $s_{k_1k_2\cdots k_n}$ are correlation parameters. Although some other forms might be simpler with fewer number of parameters, this form does provide some convenience. With Eq. 20 in which the overall Ep value is broken down into a function of individual Ep models, which are much easier to find, one does not need to worry about what form of the empirical model should be used. Also note that, if

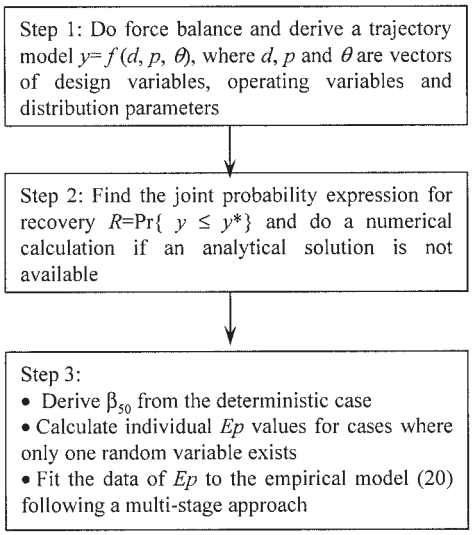

Figure 3. Diagram of the three-step approach.

any random variable K becomes deterministic (that is, Ep_K is zero), any term containing Ep_K vanishes and the model is reduced to a case with $(n-1)$ random variables. Therefore, instead of fitting the whole model at once, the parameters can actually be found by a multistage approach: first determine the values of $a_{i_1 i_2}$, $b_{i_1 i_2}$, $c_{i_1 i_2}$ by allowing only two random variables to exist; second, determine the values of $d_{j_1 j_2 j_3}$, $e_{j_1 j_2 j_3}$, $f_{j_1 j_2 j_3}$, $g_{j_1 j_2 j_3}$ by allowing three random variables to exist; and so on.

For example, with three random variables, the model looks like

$$Ep = Ep_1 + Ep_2 + Ep_3 - \frac{c_{12}}{\left(1+\frac{a_{12}}{Ep_1}\right)\left(1+\frac{b_{12}}{Ep_2}\right)} - \frac{c_{13}}{\left(1+\frac{a_{13}}{Ep_2}\right)\left(1+\frac{b_{13}}{Ep_3}\right)} - \frac{c_{23}}{\left(1+\frac{a_{23}}{Ep_1}\right)\left(1+\frac{b_{23}}{Ep_3}\right)} - \frac{g_{123}}{\left(1+\frac{d_{123}}{Ep_1}\right)\left(1+\frac{e_{123}}{Ep_2}\right)\left(1+\frac{f_{123}}{Ep_3}\right)} \quad (21)$$

Note that when any one of the three random variables becomes deterministic, model 21 is reduced to the Eq. 12 model. Therefore, the parameter values of a_{12}, b_{12}, c_{12} can be found by fixing the third random variable to a constant, and similarly for a_{23}, b_{23}, c_{23} and a_{13}, b_{13}, c_{13} by fixing the first and second random variables, respectively. After finding the values of all a_{ij}, b_{ij}, c_{ij} $(i<j)$, the parameters d_{123}, e_{123}, f_{123}, g_{123} can be found from the case with all three random variables.

A diagram of the three-step unified probabilistic approach is shown in Figure 3.

Through this systematic approach many other physical separation problems can be addressed, as described in the next section.

Applications

The first example shows that one can arrive at the first-order Eq. 3, which is applied in cases where a series of discrete events happen, through this approach.

(1) Elutriation in gas fluidized beds

A fluidized bed usually has two zones[5]: a dense bubbling phase and a dispersed phase. Solids carried in the bubble wake are partly thrown into the freeboard.

We assume the probability of the particle being caught in a bubble wake is p, and the probability of staying in the bed within time t (not caught in any bubble wake) is a binomial distribution, that is, exactly 0 success out of N Bernoulli trials $(1-p)^N$. Thus the probability of the particle entrained to the freeboard is the probability of being caught in at least one bubble wake

$$R = 1 - (1-p)^N \quad (22)$$

It is known that as $N \to \infty$, $\lim_{N\to\infty}(1-p)^N = e^{-pN}$. The above can be approximated by a Poisson process

$$R = 1 - e^{-pN} \quad (23)$$

The number of trials N is the total number of bubble burstings within time t

$$N = N_b A t \quad (24)$$

where N_b is the bubble bursting rate (that is, number of bursts per unit time per unit area), A is the cross-sectional area of the bed. N_b can be computed from

$$N_b = \frac{\gamma(u_0 - u_{mf})}{(1-f_w)V_b} \quad (25)$$

where u_0 is the superficial gas velocity and u_{mf} is the minimum fluidization velocity; f_w is the fraction of the wake volume in a bubble; V_b is the bubble volume; and γ is a function of Archimedes number. Assume the value of probability p is the ratio of the wake volume that is actually effective in throwing particles (V_{mw}) to the bed volume (V_{bed}): $p = V_{mw}/V_{bed}$. We then have

$$R = 1 - \exp\left[-\frac{\gamma f_{mw}(u_0 - u_{mf})}{H_{mf}(1-f_w)}t\right] \quad (26)$$

where $f_{mw} = V_{mw}/V_b$, $H_{mf} = V_{bed}/A$. This is exactly the same as in Smolders and Baeyens,[11] where the derivation is based on the first-order principles[12] (Eq. 3).

If we view the entrainment of particles to the freeboard as a trajectory with two discrete values, the above derivation is another example of the unified probabilistic approach.

(2) Froth flotation

The objective of this example is to show an application with three random variables. The schematic of a flotation tank is

Table 2. Ranges of Variables and Parameter Values in Regression for Froth Flotation

Hc (m)	0.4–2.0	μ_{dp} (m)	0.002–0.015
τ (s)	1–30	σ_{dp} (m)	0.0005–0.003
d_b (m)	0.001–0.005	μ_K	0.15–0.95
		σ_K	0.02–0.2
		D (m^2/s)	0.1–5.0

similar to the sink-float tank shown in Figure 2 except that there is a third phase (bubbles) and particles are fed from the lower section of the tank. Froth flotation is based on the difference of particle wettability: hydrophobic particles have a higher probability of reporting to the overflow. Froth flotation of large particles is believed to be different from that of small particles.[13] In the former, for example, the flotation of plastics,[14] more than one bubble attach to a large particle, and thus the flotation of particle depends on the aggregate density, whereas, in the latter, small particles attach to one bubble; thus the floatability is irrespective of the density or size of the particles.

In this paper, we consider the first case: flotation of large particles. Shen et al.[13] proposed a model for the particle-bubble aggregate density ρ_{pb}

$$\frac{\rho_{pb}}{\rho_p} = \frac{1.59}{1.59 + 4K\dfrac{d_b}{d_p}} \tag{27}$$

where ρ_p is the particle density; d_b and d_p are bubble diameter and particle diameter, respectively; and K is the bubble coverage percentage of the particle surface.

The behavior of the particle–bubble aggregates is similar to the particle sedimentation in the sink-float tank. Because of the various uncertainties such as conditioning and particle–bubble collisions, it is highly unlikely for particles of the same size to carry exactly the same number of bubbles; thus the parameter K is a random variable. Therefore we consider three random variables in this application:

(1) random velocity: $v \sim N(v_\infty, \sigma_v)$, where $\sigma_v = \sqrt{2D/\tau}$
(2) bubble coverage: $K \sim N(\mu_K, \sigma_K)$
(3) particle diameter: $d_p \sim N(\mu_{dp}, \sigma_{dp})$

The trajectory model is similar to that for sedimentation

$$Y = \text{sign}(\rho_l - \rho_{pb})\sqrt{3.03gd_p\left|\frac{\rho_l - \rho_{pb}}{\rho_l}\right|}\,\tau + B \tag{28}$$

where B is a random variable with normal distribution $N(0, \sqrt{2D\tau})$, and the origin of the y-axis starts from the tank bottom and the direction is upward.

Let $\beta = \mu_K$. It is easy to show that

$$\beta_{50} = \frac{1.59}{4}\frac{\mu_{dp}}{d_b}\left(\frac{\rho_p/\rho_l}{1 - \dfrac{Hc^2/\tau^2}{3.03g\mu_{dp}}} - 1\right) \tag{29}$$

An analytical solution for Ep cannot be found and thus we use the empirical model in Eq. 21.

First we determine the individual Ep values. The detailed derivation is shown in the appendix. We show only the final result in this section.

(1) For Ep_1: (only velocity distribution)

$$Ep_1 = \frac{1.59}{8}\frac{\mu_{dp}}{d_b}\left[\frac{\rho_p/\rho_l}{1 - \dfrac{(Hc + 0.6745\sqrt{2D\tau})^2/\tau^2}{3.03g\mu_{dp}}} - \frac{\rho_p/\rho_l}{1 - \dfrac{(Hc - 0.6745\sqrt{2D\tau})^2/\tau^2}{3.03g\mu_{dp}}}\right] \tag{30}$$

(2) For Ep_2: (only K distribution)

$$Ep_2 = 0.6745\sigma_K \tag{31}$$

(3) For Ep_3: (only d_p distribution)

$$Ep_3 = \frac{\beta_{75} - \beta_{25}}{2} \tag{32}$$

where

$$\beta_{75} = \frac{1.59}{4}\left[\frac{\rho_p/\rho_l}{1 - \dfrac{(Hc/\tau)^2}{3.03g(\mu_{dp} + 0.6745\sigma_{dp})}} - 1\right] \times \frac{(\mu_{dp} + 0.6745)\sigma_{dp}}{d_b} \tag{33}$$

$$\beta_{25} = \frac{1.59}{4}\left[\frac{\rho_p/\rho_l}{1 - \dfrac{(Hc/\tau)^2}{3.03g(\mu_{dp} - 0.6745\sigma_{dp})}} - 1\right] \times \frac{(\mu_{dp} - 0.6745\sigma_{dp})}{d_b} \tag{34}$$

Ranges of design and operating variables (Hc, τ, d_b) and distribution parameters (D, μ_{dp}, σ_{dp}, μ_K, and σ_K) are listed in Table 2. Following a two-stage regression approach described in the previous section, we obtained the following results: the parameter values are in Table 3, the RMSE is 0.015, and the

Table 3. Values of Model Parameters in Eq. 21 for Froth Flotation

a_{12}	0.0018	a_{13}	0.0000	a_{23}	0.1679	d_{123}	6.9838
b_{12}	0.4802	b_{13}	6.4745	b_{23}	0.3583	e_{123}	0.0593
c_{12}	0.5524	c_{13}	5.7021	c_{23}	1.7663	f_{123}	0.0856
						g_{123}	10.6837

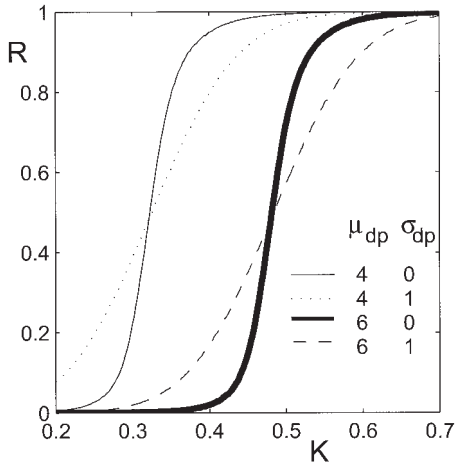

Figure 4. Partition curve for froth flotation.

μ_{dp} and σ_{dp} are in mm.

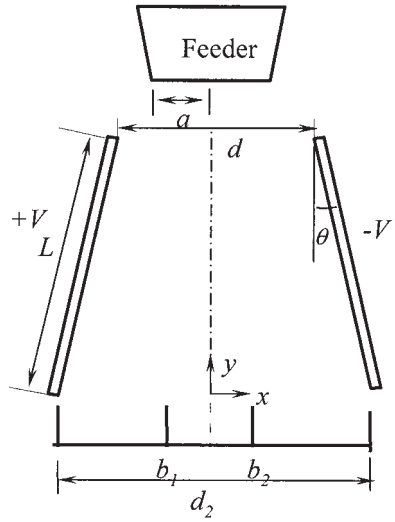

Figure 6. Free-fall electrostatic separator.

RRMSE is 3.7%.

The partition curves (recovery vs. mean bubble coverage) at different particle size distributions are shown in Figure 4. Apparently, with the same bubble coverage, it is easier to float smaller particles. Although it is impossible to find experimental data in the literature to prove our model, Figures 5a and 5b, which show the influence of particle size and flotation time on the recovery, are qualitatively consistent with Figures 7 and 10 in Shen et al.[13]

(3) Electrostatic separation

The purpose of this example is to illustrate a separation in an electrical field. Electrostatic separation, based on the difference of particle charges, can thus be used for separating particles with overlapping densities. We consider two types of separators: free-fall separators are usually used in laboratories and drum-type separators, which have larger throughput, are used industrially. In both cases, we neglect the drag force (valid for large particles in air), interparticle collisions, and influence of particle charges on the electric field.

Free-fall Separators[15]. The schematic of free-fall electrostatic separators is shown in Figure 6. The two plates, with feed gap d, end gap d_2, and length L, are inclined at angle θ and charged at constant voltage $\pm V$. Particles enter the electrical field from a feeder with feeding gap $2a$, and thus the initial position of a particle is a random variable. Three collection bins (two side bins for the products and one middle bin for the middling) are placed at the bottom with the separating positions b_1 and b_2 as indicated in Figure 6.

A second-order ODE based on Newton's second law was solved for the particle trajectory. An analytical solution for the particle horizontal position at the bottom x is

$$x = x_0 + 2\frac{A}{B}\left[\sqrt{B}\arctan\sqrt{B} - \ln\sqrt{1+B}\right] \qquad (35)$$

where $A = [(2V/d)q_m]/g$ and $B = 2\tan\theta/d$, x_0 is the initial position, and q_m is the particle charge-to-mass ratio.

In the free-fall separators, particle initial position at the top of the separator is random and assumed to have a uniform distribution $U(-a, a)$. Another random variable is the particle charge-to-mass ratio. Particle charge distribution[3] is inherent in

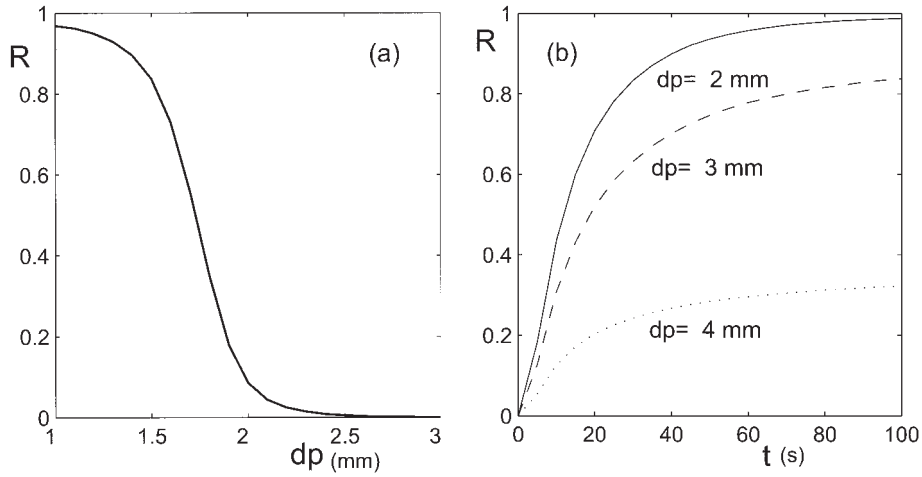

Figure 5. Influence of (a) particle size and (b) flotation time on recovery.

Table 4. Ranges of Variables and Parameter Values in Regression for Free-Fall Electrostatic Separations

M (μC kg^{-1} m^{-1})	1–50
a (m)	0–0.2
σ_q (μC kg^{-1})	0.01–4.5

the triboelectrification process because particles do not have exactly the same number of contacts with other particles. Charge-to-mass ratio is assumed to have a normal distribution: $q_m \sim N(\mu_q, \sigma_q)$.

Let $\beta = \mu_q$. The recovery to the left-side bin is then calculated from

$$r_1 = \Pr\{q_m \le (b_1 - x_0)M\} \tag{36}$$

where

$$M = \begin{cases} \dfrac{1}{\dfrac{2V}{g \tan\theta}\left[\sqrt{B}\arctan\sqrt{B} - \ln\sqrt{1+B}\right]} & \theta > 0 \\ \dfrac{gd}{2VL} & \theta = 0 \end{cases} \tag{37}$$

An analytical recovery model can then be obtained:

$$r_{1,l} = \frac{1}{2} + \frac{\Psi(g_2) - \Psi(g_1)}{2(g_2 - g_1)} \tag{38}$$

where

$$g_1 = \frac{M(b_1 - a) - \mu}{\sqrt{2}\,\sigma} \qquad g_2 = \frac{M(b_1 + a) - \mu}{\sqrt{2}\,\sigma} \tag{39}$$

and

$$\Psi(x) = x\,\mathrm{erf}(x) + \frac{1}{\sqrt{\pi}} e^{-x^2} \tag{40}$$

The Ep and cut charge for partition curve (recovery vs. mean charge-to-mass ratio) are, respectively,

$$Ep = 0.5Ma + 0.6745\sigma_q - \frac{2.8725}{\left(1 + \dfrac{1.0513}{Ma}\right)\left(1 + \dfrac{2.3784}{\sigma_q}\right)} \tag{41}$$

$$\beta_{50} = Mb_1 \tag{42}$$

with RMSE = 0.0316 and RRMSE = 2.33%.

In the derivation of β_{50} from Eq. 38, we used the following property for the error function: $erf(x) = -erf(-x)$, which leads to $g_2 = -g_1$ from $\psi(g_2) = \psi(g_1)$. Equation 42 can also be obtained directly from Eq. 36 by setting $q_m = (b_1 - x_0)M$ and the random variable x_0 to its mean value, which is zero.

The ranges of design and operating variables (M and a) and distribution parameter (σ_q) are listed in Table 4. From Eq. 42, we can see that β_{50} is linearly proportional to the collection bin position b_1. Because the recovery is a sigmoidal function of β_{50}, this means that the recovery is also a sigmoidal function of the collection bin position. This result is consistent with the experimental data (Figure 7) from Xiao et al.,[16] where the plot shows the accumulated recovery vs. the compartment number. Our result shows that particle size does not have a direct influence on the recovery. However, particle size may influence recovery by changing the charge-to-mass ratio generated by the triboelectric charging process. Further comparison is not possible because experimental data from the literature are very limited.

Drum-type Separators[17]. Figure 7 is a schematic of a drum-type separator without the tribo-electrification component. It consists of a rotating drum (partly charged with high voltage) and an outer plate (either straight or with some curvature, also charged with high voltage). Particles are transported on a belt or dropped directly from above the rotating drum. Particles detach from the drum surface if the net force (gravitational, centrifugal, and electrostatic forces) is positive in the radial direction (that is, outward). Therefore, particles that are attracted by the outer plate detach earlier and their final positions are further from the drum.

The only random variable is the charge-to-mass ratio. The following empirical trajectory model was obtained by fitting the numerical solutions of a system of 2D second-order nonlinear ODEs

$$\tilde{x}_b = b_4 \exp(b_1\tilde{x}_1 + b_2\tilde{x}_2 + b_3\tilde{x}_3) + b_5 \tag{43}$$

where b_1 to b_5 are model parameters and the ratio of electrostatic force to gravitational force, ratio of centrifugal force to gravitational force, dimensionless height of the collection bin, and dimensionless particle horizontal position are expressed, respectively, as

$$\tilde{x}_1 = \frac{-2Vq_m}{R_1 g \ln(R_2/R_1)} \tag{44}$$

$$\tilde{x}_2 = \omega^2 R_1/g \tag{45}$$

$$\tilde{x}_3 = y_c/R_1 \tag{46}$$

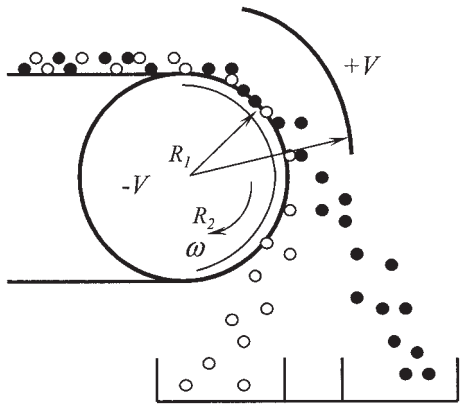

Figure 7. Drum-type electrostatic separators.

Table 5. Ranges of Variables and Parameter Values in Regression for Drum-Type Electrostatic Separations

$\tilde{x}_1$	−1.134–0.783
$\tilde{x}_2$	0.0306–0.925
$\tilde{x}_3$	−2.667–0.909
$\tilde{x}_b$	0.623–2.784

$$\tilde{x}_b = x_b/R_1 \tag{47}$$

where ω is the drum angular velocity. The variables are varied in the ranges shown in Table 5. The parameter values are in Table 6, in which the drum-type A separator has a curved outer plate (1/4 circle) that is concentric with the inner drum and the drum-type *B* separator has a straight outer plate that is assumed infinitely long and inclined at a 45° angle.

Because there is only one random variable, the derivations of the recovery model and the partition curve model are straightforward

$$r = \frac{1}{2}\left[1 - \text{erf}\left(\frac{\tilde{z} - 1}{\sqrt{2}\,\sigma_q/\mu_q}\right)\right] \tag{48}$$

where

$$\tilde{z} = \frac{\ln\left(\frac{\tilde{x}_c - b_5}{b_4}\right) - b_2\tilde{x}_2 - b_3\tilde{x}_3}{b_1\tilde{x}_1} \tag{49}$$

$$Ep = 0.6745\sigma \tag{50}$$

$$\beta_{50} = \frac{\ln\left(\frac{\tilde{x}_c - b_5}{b_4}\right) - b_2\tilde{x}_2 - b_3\tilde{x}_3}{b_1\left(\frac{-2V}{R_1 g \ln(R_2/R_1)}\right)} \tag{51}$$

As summarized in Table 7, we have shown several applications with different random variables. The trajectory models, dependent on the physics of the problem, can be analytical or empirical. When an analytical recovery model cannot be derived from the joint probability calculation, a numerical calculation is used, and numerical values of *Ep* are found to fit the expression for *Ep* directly. Even if a recovery model is analytic, the *Ep* model could still be empirical and Eq. 20 is a suggested form of the model.

Design Analysis Based on the Partition Curve

So far we have illustrated how to find the expressions for *Ep* and β_{50} values as functions of random variables, design, and operating variables. For design, we still need a simple procedure to choose the appropriate *Ep* and β_{50} values.

Consider a separation of two materials (initial fractions: f_1 and $1 - f_1$, respectively) with purity requirements ($p_1 \geq \alpha_1$ and $p_2 \geq \alpha_2$) for each product. The separation is based on the key material property β and the two materials have different values, β_1 and β_2, respectively. Our task is to find the corresponding requirements for *Ep* and β_{50} in terms of known parameters: f_1, α_1, α_2, β_1, and β_2.

The purity requirement can be formulated as

$$\begin{cases} p_1 = \dfrac{f_1 R_1}{f_1 R_1 + (1 - f_1) R_2} \geq \alpha_1 \\ p_2 = \dfrac{(1 - f_1)(1 - R_2)}{f_1(1 - R_1) + (1 - f_1)(1 - R_2)} \geq \alpha_2 \end{cases} \tag{52}$$

where R_i is the recovery of material i to product 1.

The derivation in the appendix shows that the feasible region defined by the inequalities in Eq. 52 in the two-dimensional coordinates (R_1, R_2) can be approximated by a rectangle. The decoupled requirements for R_1 and R_2 can be transformed to the following requirements for the cut points $\beta_{1,50}$ and $\beta_{2,50}$

$$\beta_1 + \gamma_1 \leq \beta_{1,50} \qquad \text{and} \qquad \beta_{2,50} \leq \beta_2 - \gamma_2 \tag{53}$$

where

$$\gamma_1 = \frac{Ep_1}{1.0986}\ln\left[\frac{\alpha_1(\alpha_2 - f_1 - 1)}{(\alpha_1 - f_1)(1 - \alpha_2)}\right]$$

$$\gamma_2 = \frac{Ep_2}{1.0986}\ln\left[\frac{\alpha_2(\alpha_2 - f_1)}{(1 - \alpha_1(\alpha_2 + f_1 - 1)}\right] \tag{54}$$

We divide the problem into two cases for simplicity of explanation.

(1) If β_{50} is a function of only design and operating variables, such as in electrostatic separation, $\beta_{1,50} = \beta_{2,50}$. In such cases, the inequalities of Eq. 53 become

$$\beta_1 + \gamma_1 \leq \beta_{50} \leq \beta_2 - \gamma_2 \tag{55}$$

The above inequalities imply a necessary condition for *Ep* values

$$\left(\frac{\alpha_1}{1 - \alpha_2}\right)^{Ep_1}\left(\frac{\alpha_2}{1 - \alpha_1}\right)^{Ep_2}\left(\frac{\alpha_2 + f_1 - 1}{\alpha_1 - f_1}\right)^{Ep_1 - Ep_2} \leq e^{1.0986|\Delta\beta|} \tag{56}$$

where $|\Delta\beta| = |\beta_1 - \beta_2|$.

The explanation for the inequalities in Eqs. 55 and 56 is that the *Ep* value (sharpness) must be less (greater) than a certain value, which is determined by the purity requirements α_1, α_2, and the difference of the material properties $\Delta\beta$. Once the *Ep* value is fixed, the cut value β_{50} must fall in an interval ($\beta_1 + \gamma_1$, $\beta_2 - \gamma_2$). Because the interval width is proportional to

Table 6. Parameter Values in Eq. 43

Separator	b_1	b_2	b_3	b_4	b_5
Drum-type A	1.6453	0.9663	−0.1251	0.5098	0.3715
Drum-type B	1.6323	1.1050	−0.1941	0.3581	0.5138

Table 7. Summary of the Models for Different Applications

	Random Variables	Trajectory Model	Recovery Model	Ep and β_{50} Models
Sink-float	Velocity, particle size	Analytical	—	Empirical
Froth flotation	Velocity, particle size, bubble coverage	Analytical	—	Empirical
Free-fall electrostatic	Initial position, particle charge	Analytical	Analytical	Empirical
Drum-type electrostatic	Particle charge	Empirical	Analytical	Analytical

$-Ep_1$ and $-Ep_2$, the smaller the Ep values are, the larger the interval is allowed. Figure 8 illustrates the feasible region for β_{50} for an example with $f_1 = 0.5$, $\alpha_1 = \alpha_2 = 0.95$, $\beta_1 = -0.477$, $\beta_2 = 0.477$, and equal Ep values ($Ep_1 = Ep_2 = 0.16$), thus satisfying the requirement in Eq. 56. From Eq. 55, the feasible interval for β_{50} is $(-0.018, 0.018)$.

For $\alpha_1 = \alpha_2$, there are three cases to consider for the relative position of the feasible interval for β_{50} between β_1 and β_2.

Case I. When $f_1 = 0.5$ and $Ep_1 = Ep_2$, $\gamma_1 = \gamma_2 = (Ep/1.0986)\ln[\alpha/(1-\alpha)]$.

When the initial fractions and Ep values are equal, respectively, the feasible interval lies in the middle between β_1 and β_2 (as in Figure 8).

Case II. When $f_1 > 0.5$ or $Ep_1 > Ep_2$, $\gamma_1 > \gamma_2$.

This can be explained from purity requirements (Eq. 52) as follows: as f_1 increases from 0.5, if β_{50} is kept the same, the purity of product 1 increases, but the purity of product 2 decreases below the requirement. To increase the purity, an efficient way is to decrease the fraction of material 1 in product 2, that is, increase the recovery of material 1 in product 1. Therefore, the interval needs to be shifted to the right at the cost of reduced recovery of material 2 in product 2. The explanation is similar for the situation when $Ep_1 > Ep_2$.

Case III. When $f_1 < 0.5$, $\gamma_1 < \gamma_2$, and the interval shifts to the left.

This can be explained similarly as in case II.

(2) β_{50} can also be a function of some material property φ, which is different for two materials, such as in sink-float separation and froth flotation, in which the cut point functions 13 and 29 contain the mean particle size. If the two materials in the feed have different mean particle size, we then have $\beta_{1,50} \neq \beta_{2,50}$. We can write $\beta_{50} = f(Q, \varphi)$, where Q is a vector of design and operating variables. After transformation, we have

$$h(\beta_1 + \gamma_1, \varphi_1) \le g(Q) \le h(\beta_2 - \gamma_2, \varphi_2) \tag{57}$$

where g and h are some functions. Therefore the inequalities of Eq. 57 define a feasible region for function $g(Q)$, and a similar analysis can be done. For example, if the two materials in a sink-float tank have different mean particle size μ_1, μ_2, using the cut point function 13 in Eq. 53, we then have

$$(\beta_1 + \gamma_1)\sqrt{3.03 g \mu_1} \le Hc/\tau \le (\beta_2 - \gamma_2)\sqrt{3.03 g \mu_2}$$

which define a feasible region for the ratio of two design variables Hc/τ.

When the design model (Eq. 53) is combined with the expressions for Ep and β_{50}, we have a very simple design procedure. We briefly illustrate this using the free-fall electrostatic separator as an example. From Eq. 41, the Ep value increases with both the standard deviation of particle charge σ_q and the value of M^*a. If any one of them is significantly greater than the upper bound (by Inequality 56), it has to be reduced. If M^*a dominates in Ep, we will have

$$\frac{\mu_{q_1}}{b_1 - \dfrac{0.5a}{1.0986}\ln\left[\dfrac{\alpha(\alpha + f_1 - 1)}{(\alpha - f_1)(1-\alpha)}\right]} \le M \le \frac{\mu_{q_2}}{b_1 + \dfrac{0.5a}{1.0986}\ln\left[\dfrac{\alpha(\alpha - f_1)}{(1-\alpha)(\alpha + f_1 - 1)}\right]} \tag{58}$$

Similarly, if σ_{q1} and σ_{q2} dominate in Ep_1 and Ep_2, we will have

$$\frac{\mu_{q_1} + \dfrac{0.6745\sigma_{q_1}}{1.0986}\ln\left[\dfrac{\alpha(\alpha + f_1 - 1)}{(\alpha - f_1)(1-\alpha)}\right]}{b_1} \le M \le \frac{\mu_{q_2} - \dfrac{0.6745\sigma_{q_2}}{1.0986}\ln\left[\dfrac{\alpha(\alpha - f_1)}{(1-\alpha)(\alpha + f_1 - 1)}\right]}{b_1} \tag{59}$$

If Ma, σ_{q1}, and σ_{q2} are in the same magnitude, one can substitute Eqs. 41 and 42 into Eq. 55 to solve quadratic equations for an upper and a lower bound of M.

The inequality constraint for M makes the design procedure fairly simple. M can be adjusted by controlling the voltage V and the plate geometry d/L, depending on which one results in a lower cost. The feasible region of M can be adjusted by moving the bin position b_1.

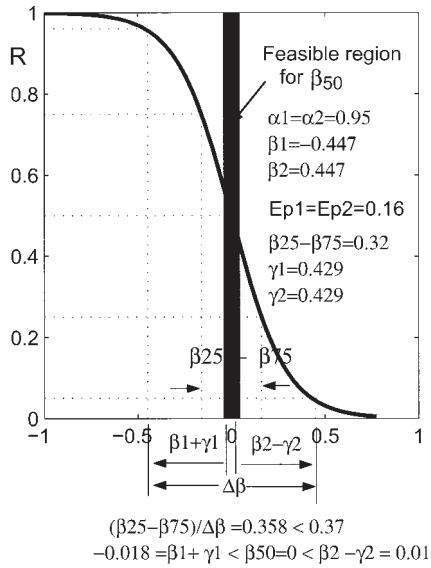

Figure 8. Illustration of the feasible region for β_{50}.

Conclusions

This paper has shown how trajectory-based solid–solid separations can be modeled with a unified approach based on a joint probability calculation of recovery, which is a departure from a traditional differential equation–based approach. One advantage of the unified approach is its ability to handle the randomness of individual particle properties. A connection between the probabilistic recovery model and the empirical partition curve model was also built that simplifies the design to a procedure that sets two parameters.

Although the probabilistic approach interprets the separations from a microscopic perspective, this does not mean macroscopic information can be eliminated. Sometimes the microscopic parameters, such as the velocity deviation or bubble coverage deviation, need to be calculated from experimentally determined macroscopic quantities such as the concentration. For example, Martin et al.[18] proposed to use a solid–liquid fluidized bed, in which the upward flowing solvent counterbalances gravity, to overcome sedimenting suspension and polydispersity problems. Thus, a steady state is obtained and the concentration profile, from which the diffusion coefficient and thus the velocity deviation can be calculated, is measured.

It should be noted that the purpose of this approach is not to simulate the exact particle trajectories. We aim to provide a simple method to develop recovery models for the unit design and optimization purpose in the context of solids separations where the separations are usually nonsharp. Therefore factors that influence the trajectories are neglected if they have insignificant effect on the recovery. Certain factors may be difficult to embed into probability calculations because of an inability to represent their influence in a succinct distribution function. In that case, one may need to use a combination of different distribution functions to represent the data accurately. The recovery models presented in the application section are used as examples of how to apply the methodology. There may be applications where changes of the assumptions for the distributions or the operation conditions invalidate the specific results. For example, a lognormal distribution may be a better representation for the particle size distribution if the feed particles come from a grinding unit. It is possible to derive the appropriate recovery models using the general approach of this paper by changing the distribution functions or the trajectory models as necessary.

Literature Cited

1. Cui J, Forssberg E. Mechanical recycling of waste electric and electronic equipment: A review. *J Hazard Mater*. 2002;99:243-263.
2. Kelly EG, Spottiswood DJ. *Introduction to Mineral Processing*. New York, NY: Wiley; 1982.
3. Lowell J, Rose-Innes AC. Contact electrification. *Adv Phys*. 1980;29: 947-1023.
4. Napier-Munn TJ. Modelling and simulating dense medium separation processes—A progress report. *Miner Eng*. 1991;4:329-346.
5. Kunii D, Levenspiel O. *Fluidization Engineering*. 2nd Edition. Boston, MA: Butterworth-Heinemann; 1991.
6. Finch JA, Dobby GS. *Column Flotation*. Elmsford, NY: Pergamon Press; 1998.
7. Ham JM, Homsy GM. Hindered settling and hydrodynamic diffusion in quiescent sedimenting suspensions. *Int J Multiphase Flow*. 1988; 14:533-546.
8. Nicolai H, Herzhaft B, Hinch EJ, Oger L, Guazzelli E. Particle velocity fluctuations and hydrodynamic self-diffusion of sedimenting non-Brownian spheres. *Phys Fluids*. 1995;7:12-23.
9. Tory EM. Stochastic sedimentation and hydrodynamic diffusion. *Chem Eng J*. 2000;80:81-89.
10. Laso M. Stochastic dynamic approach to transport phenomena. *AIChE J*. 1994;40:1297-1309.
11. Smolders K, Baeyens J, Elutriation of fines from gas fluidized beds: Mechanisms of elutriation and effect of freeboard geometry. *Powder Technol*. 1997;92:35-46.
12. Leva M. Elutriation of fines from fluidized systems. *Chem Eng Prog*. 1951;47:39-45.
13. Shen H, Forssberg E, Pugh RJ. Selective flotation separation of plastics by particle control. *Resour Conserv Recy*. 2001;33:37-50.
14. Shen H, Pugh RJ, Forssberg E. A review of plastics waste recycling and the flotation of plastics. *Resour Conserv Recy*. 1999;25:85-109.
15. Wei J, Realff MJ. Design and optimization of free-fall electrostatic separators for plastics recycling. *AIChE J*. 2003;49:3138-3149.
16. Xiao C, Allen L III, Biddle MB, Fisher MM. Electrostatic separation and recovery of mixed plastics. Report from American Plastics Council. www.plasticsresource.com/s_plasticsresource/docs/900/852.pdf; 1999.
17. Wei J, Realff MJ. Design and optimization of drum-type electrostatic separators for plastics recycling. *Ind Eng Chem Res*. 2005;44:3503-3504.
18. Martin J, Rakotomalala N, Salin D. Hydrodynamic dispersion of noncolloidal suspensions: Measurement from Einstein's argument. *Phys Rev Lett*. 1995;74:1347-1350.

Appendix

Derivation of froth flotation recovery model

In this appendix, we provide the details on the derivation of Eqs. 29–34 for the froth flotation recovery model. The derivation is based on Eqs. 27 and 28 and assumptions for the distributions of settling velocity, bubble coverage, and particle size.

First, for β_{50}, let the right-hand side of Eq. 28 equals Hc, with the random variables at their respective mean values

$$\text{sign}(\rho_l - \rho_{pb})\sqrt{3.03 g \mu_{dp}\left|\frac{\rho_l - \rho_{pb}}{\rho_l}\right|}\,\tau = Hc \tag{A1}$$

We have

$$\rho_{pb} = \left(1 - \frac{Hc^2}{3.03 g \mu_{dp} \tau^2}\right)\rho_l \tag{A2}$$

From the particle-bubble aggregate density model (Eq. 27), we find that

$$\mu_K = \frac{1.59}{4}\frac{\mu_{dp}}{d_b}\left(\frac{\rho_p/\rho_l}{1 - \dfrac{Hc^2/\tau^2}{3.03 g \mu_{dp}}} - 1\right) \tag{A3}$$

Because β is defined as the mean bubble coverage, the above gives the expression for β_{50} as shown in Eq. 29.

Next, we derive the individual E_p values.

(1) When there is only the velocity distribution

$$R = \Pr\{Y \geq Hc\} = \Pr\left\{B \geq Hc \pm \sqrt{3.03 g \mu_{dp}\left|\frac{\rho_l - \rho_{pb}}{\rho_l}\right|}\,\tau\right\}$$
$$= 1 - \frac{1}{2}\left[1 + \text{erf}\left(\frac{Hc \pm \sqrt{3.03 g \mu_{dp}\left|\dfrac{\rho_l - \rho_{pb}}{\rho_l}\right|}\,\tau}{\sqrt{2}\,\sqrt{2D\tau}}\right)\right] \tag{A4}$$

Let the right-hand side of Eq. A4 to be 0.75; we then have

$$\frac{Hc \pm \sqrt{3.03g\mu_{dp}\left|\frac{\rho_l-\rho_{pb}}{\rho_l}\right|}\,\tau}{\sqrt{2}\,\sqrt{2D\tau}} = -0.4769$$

After some rearrangement, we have

$$\rho_{pb} = \left[1 - \frac{(Hc + 0.6745\sqrt{2D\tau})^2}{3.03gdp\tau^2}\right]\rho_l \tag{A5}$$

By substituting Eq. A5 into Eq. 27, we have

$$\beta_{75} = \frac{1.59}{4}\frac{\mu_{dp}}{d_b}\left[\frac{\rho_p/\rho_l}{1 - \dfrac{(Hc + 0.6745\sqrt{2D\tau})^2/\tau^2}{3.03g\mu_{dp}}}\right] \tag{A6}$$

Similarly, when the right-hand side of Eq. A4 is set at 0.25, we have

$$\frac{Hc \pm \sqrt{3.03g\mu_{dp}\left|\frac{\rho_l-\rho_{pb}}{\rho_l}\right|}\,\tau}{\sqrt{2}\,\sqrt{2D\tau}} = 0.4769$$

Again, after some rearrangement, we obtain

$$\beta_{25} = \frac{1.59}{4}\frac{\mu_{dp}}{d_b}\left[\frac{\rho_p/\rho_l}{1 - \dfrac{(Hc - 0.6745\sqrt{2D\tau})^2/\tau^2}{3.03g\mu_{dp}}}\right] \tag{A7}$$

From the definition for Ep,

$$Ep = \frac{\beta_{75} - \beta_{25}}{2}$$

we obtain Eq. 30

$$Ep_1 = \frac{1.59}{8}\frac{\mu_{dp}}{d_b}\left[\frac{\rho_p/\rho_l}{1 - \dfrac{(Hc + 0.6745\sqrt{2D\tau})^2/\tau^2}{3.03g\mu_{dp}}} - \frac{\rho_p/\rho_l}{1 - \dfrac{(Hc - 0.6745\sqrt{2D\tau})^2/\tau^2}{3.03g\mu_{dp}}}\right]$$

(2) When there is only the bubble coverage distribution

$$R = \Pr\{Y \ge Hc\} = \Pr\left\{\pm\sqrt{3.03g\mu_{dp}\left|\frac{\rho_l-\rho_{pb}}{\rho_l}\right|}\,\tau \ge Hc\right\} = \Pr\left\{\rho_{pb} \le \left(1 - \frac{Hc^2}{3.03g\mu_{dp}\tau^2}\right)\rho_l\right\}$$

By substituting Eq. 27 into the above, we have

$$R = \Pr\left\{K \ge \frac{1.59}{4}\frac{\mu_{dp}}{d_b}\left[\frac{\rho_p/\rho_l}{\left(1 - \dfrac{Hc^2}{3.03g\mu_{dp}\tau^2}\right)} - 1\right]\right\} \tag{A8}$$

$$= 1 - \frac{1}{2}\left\{1 + \mathrm{erf}\left(\frac{\dfrac{1.59}{4}\dfrac{\mu_{dp}}{d_b}\left[\dfrac{\rho_p/\rho_l}{\left(1 - \dfrac{Hc^2}{3.03g\mu_{dp}\tau^2}\right)} - 1\right] - \mu_K}{\sqrt{2}\,\sigma_K}\right)\right\}$$

After setting $R = 0.75$, we have

$$\frac{\dfrac{1.59}{4}\dfrac{\mu_{dp}}{d_b}\left[\dfrac{\rho_p/\rho_l}{\left(1 - \dfrac{Hc^2}{3.03g\mu_{dp}\tau^2}\right)} - 1\right] - \mu_K}{\sqrt{2}\,\sigma_K} = -0.4769 \tag{A9}$$

After rearrangement, we have

$$\beta_{75} = \mu_K = \frac{1.59}{4}\frac{\mu_{dp}}{d_b}\left[\frac{\rho_p/\rho_l}{\left(1 - \dfrac{Hc^2}{3.03g\mu_{dp}\tau^2}\right)} - 1\right] + 0.4769\sqrt{2}\,\sigma_K \tag{A10}$$

Similarly, we have

$$\beta_{25} = \mu_K = \frac{1.59}{4}\frac{\mu_{dp}}{d_b}\left[\frac{\rho_p/\rho_l}{\left(1 - \dfrac{Hc^2}{3.03g\mu_{dp}\tau^2}\right)} - 1\right] - 0.4769\sqrt{2}\,\sigma_K \tag{A11}$$

Then, we obtain

$$Ep_2 = \frac{0.4769\sqrt{2}\,\sigma_K - (-0.4769\sqrt{2}\,\sigma_K)}{2} = 0.4769\sqrt{2}\,\sigma_K = 0.6745\sigma_K$$

(3) When there is only the particle size distribution

$$R = \Pr\{Y \ge Hc\} = \Pr\left\{\pm\sqrt{3.03gdp\left|\frac{\rho_l-\rho_{pb}}{\rho_l}\right|}\,\tau \ge Hc\right\} = \Pr\left\{3.03gdp\left(1 - \frac{1.59}{1.59 + 4\mu_K\dfrac{d_b}{dp}}\frac{\rho_p}{\rho_l}\right)\tau^2 \ge Hc^2\right\}$$

$$= \Pr\left\{1.59\left(\frac{\rho_p}{\rho_l} - 1\right)dp^2 - \left(4\mu_K d_b - \frac{1.59Hc^2}{3.03g\tau^2}\right)dp + \frac{4\mu_K d_b Hc^2}{3.03g\tau^2} \le 0\right\} \tag{A12}$$

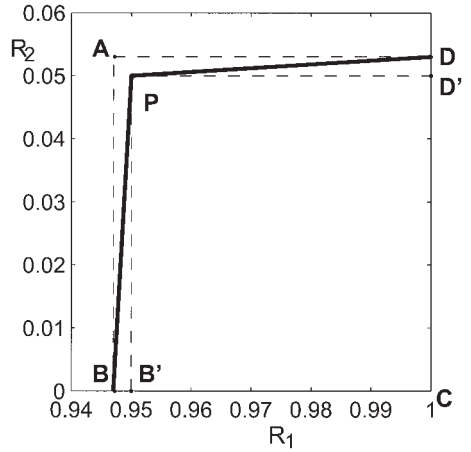

Figure A1. Feasible region for R_1 and R_2.

Let $f(\mu_K)$ represent the positive root for d_p of the above equality; then

$$R = \Pr\{dp \le f(\mu_K)\} = \frac{1}{2}\left\{1 + \mathrm{erf}\left[\frac{f(\mu_K) - \mu_{dp}}{\sqrt{2}\,\sigma_{dp}}\right]\right\} \quad \text{(A13)}$$

Set $R = 0.75$; we then have

$$f(\mu_K) = \mu_{dp} + 0.6745\sigma_{dp} \quad \text{(A14)}$$

Because $f(\mu_K)$ is the root for the quadratic function in Eq. A12, we substitute d_p by $\mu_{dp} + 0.6745\sigma_{dp}$ in the equality of A12; then we have

$$\beta_{75} = \mu_K = \frac{1.59}{4}\left[\frac{\rho_p/\rho_l}{1 - \dfrac{(Hc/\tau)^2}{3.03g(\mu_{dp} + 0.6745\sigma_{dp})}} - 1\right] \times \frac{(\mu_{dp} + 0.6745\sigma_{dp})}{d_b}$$

Similarly, we have

$$\beta_{75} = \mu_K = \frac{1.59}{4}\left[\frac{\rho_p/\rho_l}{1 - \dfrac{(Hc/\tau)^2}{3.03g(\mu_{dp} - 0.6745\sigma_{dp})}} - 1\right] \times \frac{(\mu_{dp} - 0.6745\sigma_{dp})}{d_b}$$

By definition, Ep_3 is half of the difference between β_{75} and β_{25}.

Derivation of Eqs. 53 and 54

In Figure A1, the line PB represents a contour for $p_1 = \alpha_1 = 0.95$, and the line PD represents a contour for $p_2 = \alpha_2 = 0.95$. The quadrilateral PBCD is the feasible region defined by constraint 52 for R_1 and R_2. The coordinates of the points B, D, and P are

$$R_1(B) = \frac{\alpha_2 + f_1 - 1}{\alpha_2 f_1} \qquad R_2(B) = 0$$

$$R_1(D) = 0 \qquad R_2(D) = \frac{f_1(1 - \alpha_1)}{(1 - f_1)\alpha_1}$$

$$R_1(P) = R_1(B') = \frac{\alpha_1(\alpha_2 + f_1 - 1)}{f_1(\alpha_1 + \alpha_2 - 1)}$$

$$R_2(P) = R_2(D') = \frac{(1 - \alpha_1)(\alpha_2 + f_1 - 1)}{(1 - f_1)(\alpha_1 + \alpha_2 - 1)}$$

It can be shown that, if $1 - \alpha_2 \le f_1 \le \alpha_1$ and $\alpha_1 + \alpha_2 - 1 > 0$, we have

$$\Delta B = R_1(B') - R_1(B) = \frac{(1 - \alpha_1)(1 - \alpha_2)(\alpha_2 + f_1 - 1)}{\alpha_2 f_1(\alpha_1 + \alpha_2 - 1)} \ge 0$$

and

$$\Delta D = R_2(D) - R_2(D') = \frac{(1 - \alpha_1)(1 - \alpha_2)(\alpha_1 - f_1)}{\alpha_1(\alpha_1 + \alpha_2 - 1)(1 - f_1)} \ge 0$$

It can also be shown that for α_1, $\alpha_2 \ge 0.95$, $\Delta B_{max} = 0.00277$ and $\Delta D_{max} = 0.00277$. Because ΔB and ΔD are sufficiently small, the rectangle PB′CD′ is a good approximation to the feasible region PBCD. Thus the constraints of Eq. 52 are decoupled to

$$R_1 \ge \frac{\alpha_1(\alpha_2 + f_1 - 1)}{f_1(\alpha_1 + \alpha_2 - 1)} \qquad \text{and} \qquad R_2 \le \frac{(1 - \alpha_1)(\alpha_2 + f_1 - 1)}{(1 - f_1)(\alpha_1 + \alpha_2 - 1)}$$

Note that, although two materials are separated in the same separator, they may have different partition curve models. Let Ep_1, $\beta_{1,50}$ and Ep_2, $\beta_{2,50}$ be the Ep and β_{50} values for material 1 and material 2, respectively.

From

$$\exp\left[\frac{1.0986}{Ep_1}(\beta_1 - \beta_{1,50})\right] = \frac{1}{R_1} - 1 \le \frac{1}{\dfrac{\alpha_1(\alpha_2 + f_1 - 1)}{f_1(\alpha_1 + \alpha_2 - 1)}} - 1 = \frac{(\alpha_1 - f_1)(1 - \alpha_2)}{\alpha_1(\alpha_2 + f_1 - 1)}$$

we have $\beta_{1,50} \ge \beta_1 + \gamma_1$, where

$$\gamma_1 = \frac{Ep_1}{1.0986}\ln\left[\frac{\alpha_1(\alpha_2 + f_1 - 1)}{(\alpha_1 - f_1)(1 - \alpha_2)}\right]$$

Similarly from

$$\exp\left[\frac{1.0986}{Ep_2}(\beta_2 - \beta_{2,50})\right] = \frac{1}{R_2} - 1$$

$$\geq \frac{1}{\dfrac{(1-\alpha_1)(\alpha_2 + f_1 - 1)}{(1-f_1)(\alpha_1 + \alpha_2 - 1)}} - 1 = \frac{\alpha_2(\alpha_1 - f_1)}{(1-\alpha_1)(\alpha_2 + f_1 - 1)}$$

we have $\beta_{2,50} \leq \beta_2 - \gamma_2$, where

$$\gamma_2 = \frac{Ep_2}{1.0986} \ln\left[\frac{\alpha_2(\alpha_1 - f_1)}{(1-\alpha_1)(\alpha_2 + f_1 - 1)}\right]$$

Manuscript received Nov. 12, 2003, and revision received Jan. 6, 2005.